

PRECIPITATION MECHANISMS IN NON-FERROUS ALLOYS

Precipitates Dissolution, Phase Transformation, and Re-precipitation-Induced Hardness Variation in 6082-T6 Alloy During MIG Welding and Subsequent Baking

WENKANG ZHANG,¹ HONG HE,^{1,2} CONGCHANG XU,¹
WANYU YU,¹ and LUOXING LI¹

1.—State Key Laboratory of Advanced Design and Manufacturing for Vehicle Body, College of Mechanical and Vehicle Engineering, Hunan University, Changsha 410082, People's Republic of China. 2.—e-mail: hehong_hnu@hnu.edu.cn

Precipitation evolution-induced hardness variation in 6082-T6 alloy during various thermal histories of welding and subsequent paint baking was characterized systematically. Precipitation evolution in various subzones of the heat-affected zone (HAZ) from the weld toe to the base materials was precisely identified by transmission electron microscopy. Under heating processes of welding and baking with different temperature and time duration, the morphology evolution of precipitates comprised dissolution, coarsening in size, and phase transformation from β'' to $U2$, β' and β , etc. The mechanisms of the thermal softening and bake hardening of mechanical properties in HAZ are clarified. Quantitative calculation results showed that grain growth contributed little to the strength loss in HAZ, while precipitate evolution was responsible. Re-precipitating of Guinier–Preston zones and β'' phase from the super-saturated solid solution produced by welding was found to make main contributions to the efficient hardness recovering of joints during post-weld paint baking.

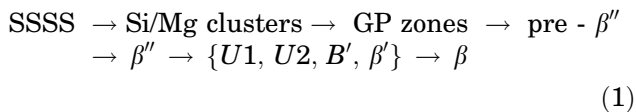
INTRODUCTION

The heat-treatable Al-Mg-Si alloys have been extensively used in the automotive industry as lightweight materials due to their desirable combination of low density, high strength-to-weight ratio, excellent workability and weldability, and superior corrosion resistance.¹ In their wide application as structural materials, welding is the main connecting technique but with enormous challenges. Until now, the tungsten inert gas (TIG), metal inert gas (MIG), and friction stir welding (FSW) are the most widely used welding methods for aluminum alloys. Among these welding techniques, the MIG welding is the most popular method adopted in the automobile production process owing to its comparatively easier applicability, high efficiency, and relatively low cost.² However, because of microstructure evolution (e.g., grain growth and/or precipitation evolution), the strength softening in some subzones of the welded joints caused by thermal input during welding, which are called “heat affected zones”

(HAZ), makes light weighting difficult.³ Fortunately, such a strength loss can be recovered during their subsequent paint baking process through additional precipitation strengthening. Nevertheless, the microstructure evolution including the precipitates dissolution, phase transformation, and re-precipitation during welding and subsequent baking is complicated but is usually not so precisely characterized yet. Therefore, a systematic study, aiming to understand the precipitation evolution and its influence on mechanical properties of Al-Mg-Si alloys during multistage heating processes of MIG welding and subsequent paint baking, is of highly scientific significance.

Thermal softening of the welded Al-Mg-Si alloy has been widely reported and proved to be highly related to the microstructure evolution under various thermal histories of welding. The temperature rising in the HAZ leads to the significant variation of the microstructure and mechanical properties. The reasons for this influence comprise grain growth and precipitation decomposition. It is

generally accepted that the strength of materials decreases as the grain size increases, which results in a smaller grain boundary amount.^{4,5} Therefore, grain growth in some locations in the welded joint induced by heating has always been considered to be one reason for degradation of mechanical properties. In the case of heat-treatable Al-Mg-Si alloys, the precipitation evolution including the precipitate coarsening and phase transformation during welding is another essential factor. Yan et al.⁶ found that in the Al-Mg-Si alloys, the grain growth together with precipitation evolution contributes to strength loss during welding. However, how much weight does each aspect contribute to the strength loss is still ambiguous and desires further quantitative analysis. Diverse precipitation evolution processes would occur in the HAZ of Al-Mg-Si alloys during welding because the temperature in these zones varies in the range of the thermal treatment temperatures of these alloys. As a result, the morphology including phase type, particle size, and distribution of the precipitates and their strengthening effects would be significantly influenced. The general precipitation sequence for the Al-Mg-Si alloys is as follows:⁷



where SSSS is the super-saturated solid solution, GP (Guinier–Preston) zones are aggregates of solute atoms embedded in the Al matrix, and other symbols represent different precipitate phases. Among these precipitates, the β'' phase has been proved to be the most effective strengthening precipitate for Al-Mg-Si alloys in T6 temper.⁸ Except for the equilibrium phases β -Mg₂Si, all other phases are metastable that might incline to dissolve or transform into another phase in diverse thermal conditions. Benoit et al.⁹ investigated the relationship between the hardness changes and precipitation evolution in the HAZ of 6061-T6 MIG-welded joints through transmission electron microscopy (TEM). It was demonstrated that softening of the HAZ was attributed to the lowered density of β'' precipitates and the presence of β' phase with a larger size, which has a smaller strengthening effect. However, these studies lacked strong evidence to confirm detailed characteristics of diverse phases, and at which temperatures these transformations take place. Therefore, the microstructural development of the precipitates corresponding to the thermal histories of welding and resultant mechanical property evolution stays unclear. Although thermal softening occurs unavoidably during welding, the strength of the welded Al-Mg-Si joints in practical applications would have chance to be partially recovered, through subsequent manufacturing processes such as post-weld storage, thermal machining, and paint baking.¹⁰ These short-time heating

processes are equal to additional artificial aging treatments to the joints. The typical paint baking process designed for automotive body sheets comprises at least three times heating such as primer, paint, and varnish at 170°C to 180°C for 20 min to 30 min per cycle. The positive effect of paint baking on precipitation hardening in Al-Mg-Si alloys after quenching from the solution treatment temperature has been well demonstrated. For example, Chen et al.¹¹ reported that after one cycle of post-weld paint baking, both the fusion zone and the HAZ produced by friction stir spot welding were found to become harder than the parent 6111-T4 sheet. Nevertheless, little attempt has been made for more precise identification of the re-precipitation behavior in the detailed subzones of the welded joints.

To explore these lingering problems further, the objective of the present work is to conduct a detailed microstructural study about the systematical characterization of the precipitation evolution process under multistage heating processes of MIG welding and subsequent paint baking. Commercial 6082-T6 Al-Mg-Si alloy was adopted. The accurate correspondence between thermal histories, precipitation evolution, and mechanical properties in diverse subzones from the base material (BM) to the weld seam was established by means of temperature monitoring, hardness measurements, and TEM analysis. Grain growth and precipitation evolution in subzones of the HAZ were studied. In addition, precipitation evolution during post-weld paint baking was discussed to interpret the recovering mechanism.

EXPERIMENTAL DETAILS

A commercial 6082-T6 extruded profile with dimensions of 200 × 150 × 4 mm and 5356 aluminum welding wire with 1.2 mm in diameter were used as the raw materials. Their chemical compositions were 0.74 Mg-0.88Si-0.42Mn-0.21Fe-balance Al and 5.25 Mg-0.25Si-0.03Mn-0.39Fe-balance Al in weight percent (wt.%), respectively. Butt weld workpieces were obtained using a Kemppi FAS-TMIG PULSE 450 MIG welding machine equipped on an auto manipulator. Argon with purity of 99.999% was used as the shielding gas. MIG welding parameters adopted were 165 A, 20 V, and 65 cm min⁻¹, respectively. The thermal history of subzones in the welds with different distances from the welding seam center to the BM was real time monitored and recorded by several type-K thermocouples. Each thermocouple was inserted into a hole with a diameter of 1.0 mm and 2.5 mm in depth drilled in a line perpendicular to the seam from the surface.

Simulated paint baking was conducted on samples by heating at 175°C with the duration of 30 min for 1 to 3 cycles. It should be noted that the time of 30 min includes the heating time estimated to be 5 min to 10 min, and thereafter the keeping time is

20 min to 25 min. Hardness of different samples before and after baking were measured on the upper surfaces of polished samples, conducted on a HY 1000-A type Vickers hardness testing machine under a load of 1 kg and a duration time of 15 s. Tensile tests were performed by a uniaxial tensile testing method according to ASMT standards E8 M-09. Standard dumbbell-type tensile specimens with the welds in the center and a gauge length of 100 mm and width of 12.5 mm were used. Tests were conducted on an INSTRON-3382 tensile testing machine with stretching speed of 1 mm min⁻¹. All mechanical properties testing were performed at room temperature.

Grain size measurements and precipitate morphology of the cross section of the welded joints were examined by TEM and high-resolution transmission electron microscopy (HRTEM). Specimens for TEM were slowly sliced perpendicular to the seam to about 2 mm in thickness by Wire Cut Electrical Discharge Machining from different subzones of the joint, i.e., the BM, weld toe, and HAZ. All these specimens were first mechanically ground to about 100 μm in thickness and then further thinned by twin-jet electropolishing with a solution of 30 vol.% nitric acid and 70 vol.% methanol at -25°C, 18 V, and 80 mA. TEM observations were performed on a Tecnai F20 TEM system (FEI, Hillsboro, OR, USA) operated at 200 kV. Observation of TEM is repeated on at least five points for each sample.

RESULTS

Hardness Distributions of the As-Welded Joint

The hardness distributions of the as-welded joint produced by using 6082 BM and 5356 filler metal were analyzed immediately after welding. Figure 1 presents the corresponding relationship between the schematic image and as-welded hardness values

measured within 2 h. The weld structure is divided into detailed subzones including the fusion zone, weld toe, HAZ, and BM, as conventionally named. The hardness of them differs remarkably. Hardness of the BM is about 110 HV₁, while those for the HAZ decrease gradually to the lowest value of 60 HV₁ from the BM to weld toe. A bump to around 85 HV₁ is observed in the weld toe. The values for the fusion zone are about 70 HV₁ and show a smooth trend within this region.

From the hardness curve as shown in Fig. 1b, it is obvious that significant softening behavior has occurred in the welded joints, particularly in the HAZ. The HAZ is located in the region with a distance of 5 mm to 13 mm to the center of the weld seam, and the weakest region locates in the range of 6 mm to 10 mm to the center. The fusion zone with a width of 8 mm shows gently fluctuated hardness and a little higher than that of the weakest region of HAZ.

Mechanical Properties of Joints After Paint Baking

The mechanical properties of the as-welded joint after various typical baking cycles at 175°C were investigated, as shown in Fig. 2. It can be observed that baking cycles can efficiently recover the hardness of the welded joint in the subzones of the weld seam, weld toe, and HAZ. Nevertheless, it should be noted that after the completion of three baking cycles, the degree of hardness recovery of each region is different, showing diverse baking responses as the distance to the weld center increases. The hardness of the fusion zone was raised by 12 HV₁ after the third baking cycle. The maximum increase of hardness (~30 HV₁) occurred in the weld toe, which has reached up to the level of BM (110 HV₁) after the completion of the third baking cycles, indicating the greatest baking response. In the HAZ, the baking response also shows improvements in hardness but with the gradually weakened effect as the distance to the weld center increases. In the regions with distance 6 mm to 8 mm to the weld center line, the average increase in hardness after three baking cycles is about 26 HV₁. As the distances increased to 8 mm to 10 mm, the average increase of hardness is only about 14 HV₁, indicating a much weaker baking response.

To investigate further the enhancement of mechanical properties after baking, tensile tests of the welded joints with different baking time were conducted. Figure 2b shows the overall tensile strength of the welded joints after different baking cycles, with a comparison to that of the BM. When tested immediately after welding (within 2 h), the strength showed a loss by 44% compared with the BM due to welding. The tensile strength increased by 25 MPa, 47 MPa, and 62 MPa after each baking cycle, respectively. The strength coefficient was

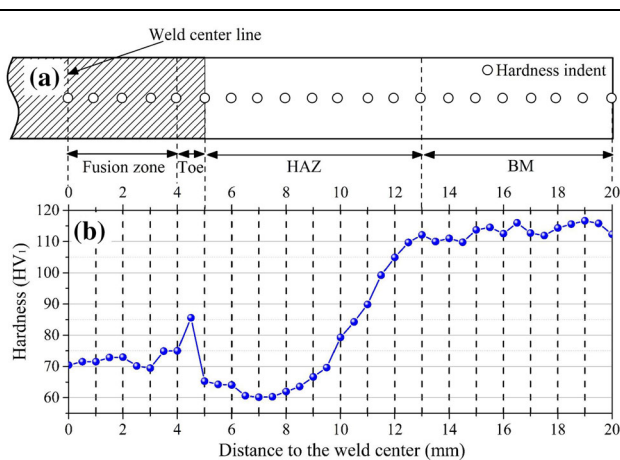


Fig. 1. Corresponding relationship of as-welded hardness and schematic image of the MIG weld: (a) schematic image of the upper surface of welded joint and (b) distributions of hardness along the direction perpendicular to the weld center.

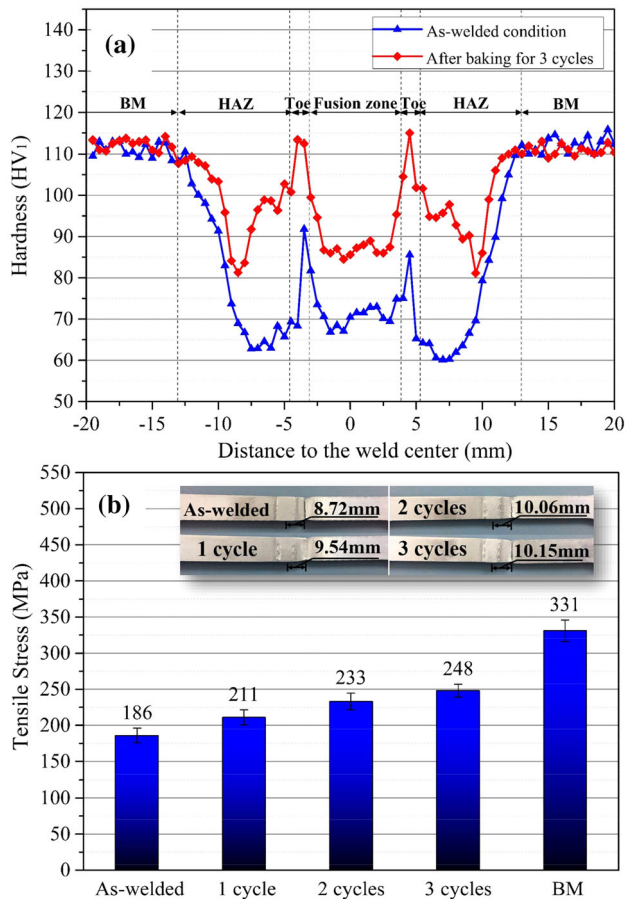


Fig. 2. Changes of mechanical properties of as-welded joints after typical baking cycles: (a) typical hardness change of as-welded joints after baking for three cycles at 175°C and (b) tensile strength of as-welded joints after baking for one to three cycles compared to the 6082-T6 BM. The inset figure shows the fracture locations of corresponding tensile specimens.

increased from 0.56 to 0.75 after three baking cycles. As shown in Fig. 2b, all the testing specimens fractured in the HAZ and the distances of fractured locations to the weld center were in the range of 9.21 mm to 10.15 mm. According to the percentages of elongation of the specimens in the as-welded condition (10.31%) and after three baking cycles (6.25%), the weakest location of each specimen before tensile testing can be inferred to be 7.93 mm and 9.55 mm to the weld center, respectively. These results can be supported by the hardness distributions (Fig. 2a), which show that the points of the lowest hardness value are in agreement with the tensile failure locations.

DISCUSSION

Mechanisms of Thermal Softening During Welding

The HAZ, as mentioned earlier, is the region with the weakest mechanical properties of the welded

joints with or without baking. Thus, a sufficient understanding of the softening mechanism of the HAZ is critical to obtain high-quality welded joints for industrial applications. During the MIG welding process, different microstructural changes resulted from various thermal histories are likely to take place in the HAZ. Grain growth and precipitation evolution, alone or together, have been reported to be the reasons for thermal softening of the HAZ. The present study was conducted for the purpose of verifying the main mechanism of thermal softening behavior in detailed subzones in the HAZ.

Thermal Histories During MIG Welding

The variations of the hardness in the detailed subzones from the weld seam to the BM in a joint are closely related to different thermal experiences during welding and resultant microstructure. Figure 3a and b shows distributions of measured temperature during welding as a function of time and distance to the weld seam, respectively. It can be seen that, during the welding process, the peak temperatures of different subzones vary from 650°C to 200°C as the distance changes from 5 mm to 20 mm. The heating and cooling rates were estimated. For instance, they are 63°C s⁻¹ and 26°C s⁻¹ in the HAZ (6 mm to the weld center), respectively. The subzone of HAZ (7 mm to the weld) experienced heating rate of 58°C s⁻¹ and a cooling rate of 23°C s⁻¹. It is worth noting that, as the distance to weld center increases, the peak temperature, heating, and cooling rates decrease accordingly. For example, the highest peak temperature of the weld toe can reach up to 650°C, and the heating and cooling rates of this subzone are 74°C s⁻¹ and 33°C s⁻¹, respectively.

Since the Al-Mg-Si alloy is a kind of heat-treatable aluminum alloy, heating at high temperatures affects the microstructure and mechanical properties of this alloy greatly. The highest temperature when welding varies from the melting point of the aluminum alloy (660°C)¹² to room temperature. The subzones of the HAZ experience high temperatures and quick cooling to room temperature, which equals a solutionization process. The peak temperatures of some subzones (i.e., 6 mm to 7 mm to the weld center) even exceed the solution temperature (as always considered to be 480°C or higher). These extreme changes of temperature may influence the microstructure of the welded joints significantly. Therefore, the welded joints, particular in the HAZ, exhibit different degrees of softening behavior compared with the BM after welding. In the weld toe, it is not difficult to understand that it would be strengthened by a solid solution hardening mechanism after welding. It may have been subjected to sufficient heating and fast cooling processes considered as additional solid solution and quenching treatments for the welds, which produced a super-saturated solid solution.¹³

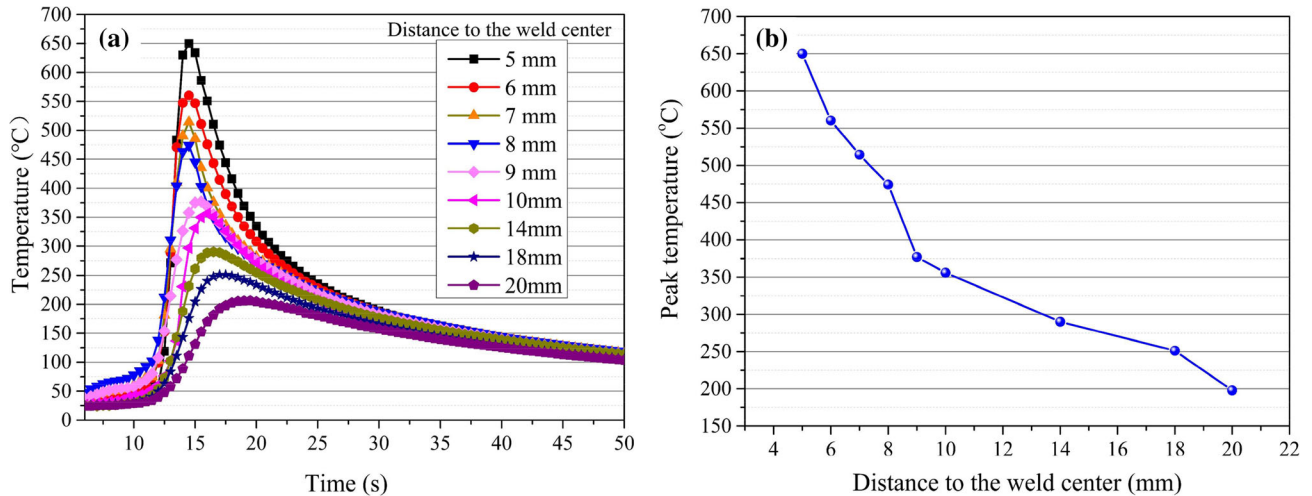


Fig. 3. Welding thermal histories measured by thermocouples: (a) temperature histories at various locations along the direction perpendicular to the weld center and (b) peak temperature distributions at various locations.

Effect of Grain Growth on Thermal Softening

It is generally accepted that grain growth in the HAZ is a non-negligible factor that should be taken into consideration when referring to the strength loss of aluminum alloy welded joints.¹⁴ To determine quantitatively the effect of grain growth on the softening of the HAZ, the accurate measurement of grain size in the HAZ (7 mm to the weld) and BM was carried out by TEM. The average grain size in the HAZ and BM is 9.65 μm and 7.73 μm , respectively.

Based on the Hall–Petch equation,^{15,16} the contribution of the grain boundary strengthening for blocking dislocation movement in the HAZ and BM of 6082-T6 MIG welded joints can be calculated, respectively, as follows:

$$\sigma_d = k_y d^{-1/2} \quad (2)$$

where d is the average grain size and k_y is a positive constant of yielding associated with the stress required to extend dislocation activity into adjacent unyielded grains. Then, because of the proportional relationship between the yield strength and hardness through the expression $H_v \approx 0.33\sigma_y$,¹⁷ the Eq. 2 could be rewritten as follows:

$$H_{vd} = k_H d^{-1/2} \quad (3)$$

where k_H is an appropriate constant associated with the hardness measurements and can be considered to be 50 $\text{HV}_1 \mu\text{m}^{1/2}$ for aluminum alloys.¹⁸ Using the grain size data, the contribution of grain boundary strengthening was calculated. The hardness contribution to the HAZ and BM is 16.09 HV_1 and 17.98 HV_1 , respectively. As stated, the average grain size of the HAZ is larger than that of the BM, indicating that grain growth did occur in the HAZ. However, only a 1.9- HV_1 decrease of the grain boundary

strengthening contributing to the HAZ hardness was found, while the results obtained from Fig. 1b show a loss of hardness by 50 HV_1 compared with the BM. From these results, it can be concluded that grain growth is not a major cause of strength loss in the HAZ.

Effect of Precipitation Evolution on Thermal Softening

To gain a better understanding of precipitation evolution in HAZ, the region with weakest hardness (6 mm to 10 mm from the weld center) was selected for a further investigation through TEM observation. This region was divided into three subzones, designated as HAZ(I), HAZ(II), and HAZ(III), with distances 8 mm to 10 mm, 7 mm to 8 mm, and 6 mm to 7 mm to the weld center, respectively. The morphology images of the precipitates in these subzones and the BM were analyzed and compared, as shown in Figs. 4, 5, 6 and 7.

Figure 4a is the TEM micrograph showing the morphology of the 6082-T6 BM viewing from the $[001]_{\text{Al}}$ direction. The inset figure in the TEM micrograph shows the corresponding selected area diffraction patterns (SADPs). As can be verified by the SADP image, all images were obtained in the direction along the $\langle 001 \rangle$ zone axis of the Al matrix. Many needle-shaped β'' precipitates are found in this region. The β'' precipitates lay homogeneously along the $\langle 100 \rangle_{\text{Al}}$ directions with 21.1 nm to 100.4 nm in length and 3.9 nm to 4.2 nm in diameter. The dark spots are needle-shaped β'' precipitates pointing in the viewing directions. Figure 4b shows the corresponding HRTEM image under the $[001]_{\text{Al}}$ zone axis. As can be seen, β'' precipitates are coherent along the needle direction (b -axis) with the $\langle 100 \rangle_{\text{Al}}$ direction, suggesting that their cell parameter is similar to Al matrix. The β'' phase was reported to be the

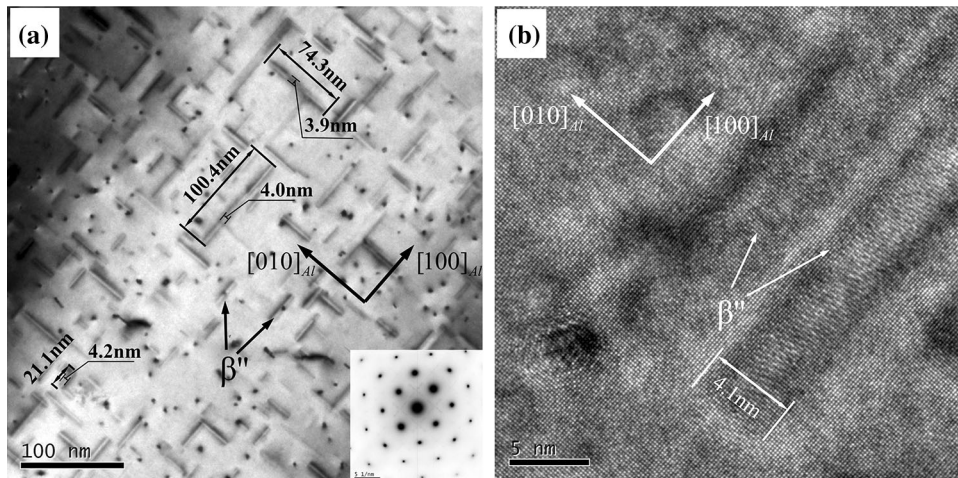


Fig. 4. TEM micrograph (a) and the corresponding HRTEM image (b) under $[001]_{Al}$ zone axis of the BM of the 6082-T6 welded joint.

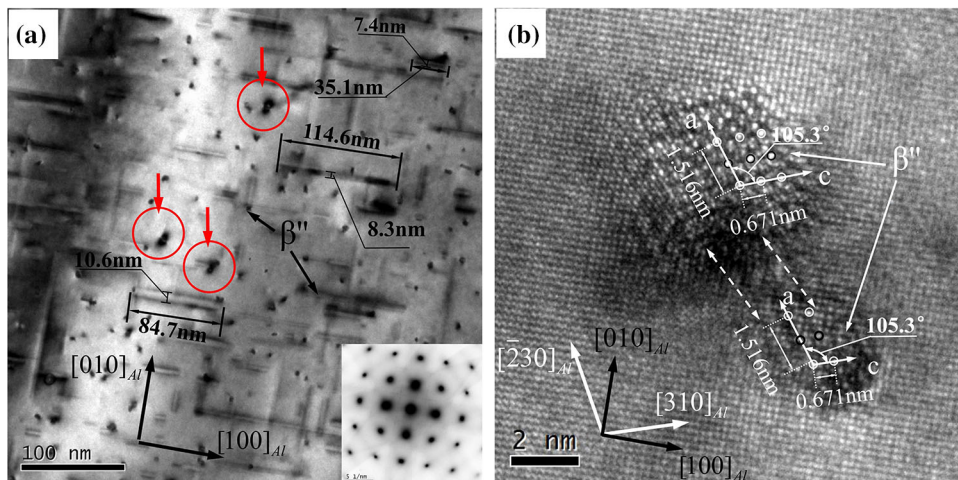


Fig. 5. TEM micrograph (a) and HRTEM image (b) under the $[001]_{Al}$ zone axis of the HAZ (I) (356°C to 474°C) of the welded joint.

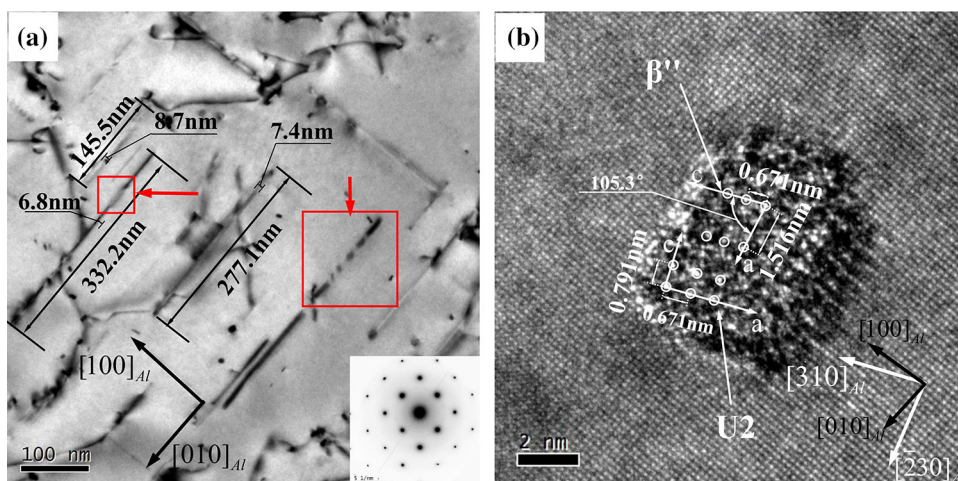


Fig. 6. TEM micrograph (a) and HRTEM image (b) under the $[001]_{Al}$ zone axis of the HAZ (II) (474°C to 514°C) of the welded joint.

monoclinic structure with $a = 0.1534 \pm 0.012$ nm, $b = 0.405$ nm, $c = 0.683 \pm 0.015$ nm, and $\beta = 106 \pm 1.5^{\circ}$.¹⁹ These fine precipitates of high-

number densities are widely recognized as the main strengthening phase formed during artificial aging.

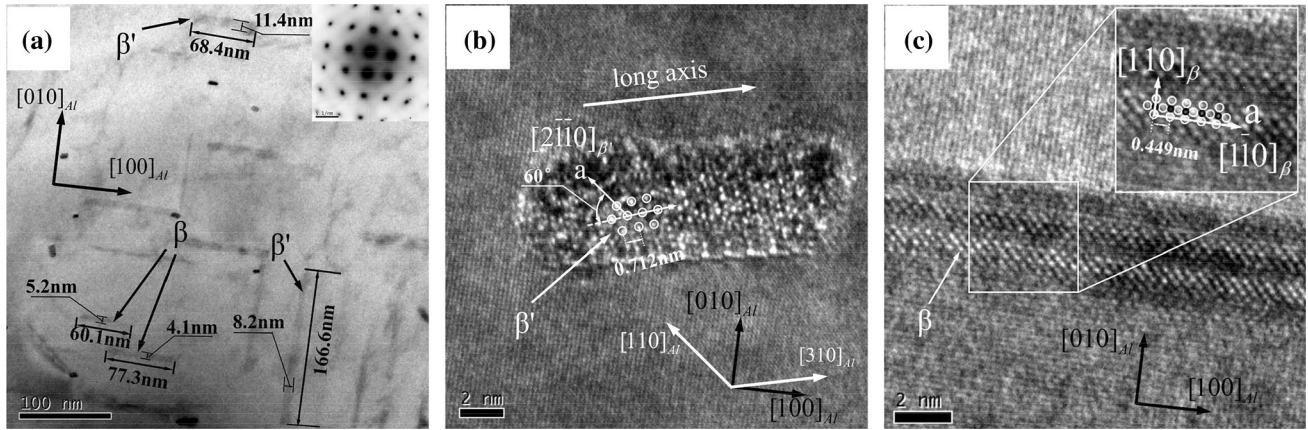


Fig. 7. TEM micrograph (a) and HRTEM images (b), (c) under the $[001]_{Al}$ zone axis of the HAZ (III) (514°C to 560°C) of the welded joint.

Figure 5 shows the precipitation evolution of HAZ(I) that occurred during welding, where it suffered to temperatures of 356°C to 474°C . As can be seen in Fig. 5a, the number of short needle-like precipitates is apparently reduced and partially replaced by precipitates with a larger size distributed unevenly along the $\langle 100 \rangle_{Al}$ direction. The size is about 35.1 nm to 114.7 nm in length and 7.4 nm to 10.6 nm in diameter. The phase type still stays in the form of the β'' phase, with the lattice parameter identified as monoclinic $a = 0.152$ nm, $c = 0.671$ nm, and $\beta = 105^{\circ}$ (Fig. 5b). This phenomenon suggests the appearance of growth and coarsening of precipitates generally considered to be from overaging.²⁰

An interesting phenomenon is that the growing in the size of the β'' phase was clearly observed. Two adjacent precipitates pointing in the observing direction are found to be in a combined state (as marked by red circles in Fig. 5a). This phenomenon was further illustrated by the corresponding HRTEM image with two adjacent precipitates. The unit cell structure and orientations are outlined in these particles, respectively. And the orientation relationship of the β'' phase with respect to the Al matrix, according to the observed results, can be described as follows:

$$(010)_{\beta''} \parallel (001)_{Al}, [100]_{\beta''} \parallel [\bar{2}30]_{Al}, [001]_{\beta''} \parallel [310]_{Al} \quad (4)$$

Moreover, it can be seen that the two β'' particles are adjacent to each other and the phase boundaries of them are already at intersection, which might indicate the occurrence of combination and growth. This is supported by the apparent increase in cross-section size and the slight increase in length of β'' precipitates in Fig. 5a. A possible explanation for this is that solid diffusion occurs between two adjacent β'' precipitates. Diffusion in solids generally depends strongly on the temperature, which is slow at low temperatures but appreciable at high temperatures.²¹ Due to the higher peak

temperature (356°C to 474°C) produced by MIG welding, the short precipitates combined with each other and grow up through diffusion, which results in a reduction in the total number and then decreases the strengthening effect. Therefore, the mechanism for softening of HAZ(I) should be the coarsening of precipitates by swallowing up smaller ones.

The subzone of HAZ(II) experienced even higher peak temperature (474°C to 514°C) compared with HAZ(I). The results of mechanical properties tests show that the tensile failure location of the as-welded joint is 7.93 mm from the weld center. Therefore, the mechanical properties of HAZ(II) are the worst of the three subzones of the HAZ. This can be explained from the aspect of precipitation evolution. As can be seen in Fig. 6a, there is a large drop in number density of precipitates. The short needle-like β'' phases with less than 50 nm in length have disappeared completely, and only a small number of long needle-like precipitates with 145 nm to 332 nm in length and 6.82 nm to 7.38 nm in diameter remain in this region. It suggests that dissolution and phase transformation might have occurred. Although the dissolution of strengthening precipitates in HAZ is a common phenomenon that has been already reported, the specific behavior of dissolution that resulted from high temperatures during welding remains unclear. An unanticipated finding from Fig. 6a is that typical long precipitates break in the middle into several parts (marked by the two red rectangles). It can be speculated that β'' phases may begin to be disintegrated from the middle and gradually dissolved through the out-diffusion of atoms from precipitates to Al matrix caused by welding. Meanwhile, the internal phase transformation from β'' phase to U_2 phase can be observed in HAZ(II). The HRTEM image shows the cross section of a coarse needle under the $[001]_{Al}$ zone axis. It is interesting to find that the needle consists of the two precipitates, β'' and U_2 , as shown in Fig. 6b. The unit cell structure and orientations of these phases are both outlined in

these particles. The $U2$ phase has a slightly different unit cell from β'' : orthorhombic, $a = 0.671$ nm, $c = 0.791$ nm, and its corresponding orientation relationship with β'' can be described as follows:

$$(010)_{U2} \parallel (001)_{Al}, [100]_{U2} \parallel [310]_{Al}, [001]_{U2} \parallel [\bar{1}30]_{Al} \quad (5)$$

$$(010)_{U2} \parallel (010)_{\beta''}, [100]_{U2} \parallel [001]_{\beta''}, [\bar{1}30]_{U2} \parallel [100]_{\beta''} \quad (6)$$

These relationships are basically coincident with the results observed by Andersen et al.,²² who suggested that $U2$ may be obtained from β'' by replacing Mg and Si atoms with Al and rearranging the atoms so that columns stack differently. This phenomenon was also reported by Granholt²⁰ who observed that cross-sectional dimensions of β'' particles in Al-Mg-Si alloys would increase as the internal transformation from β'' to $U2$ proceeds at the overaging temper. In addition, it was found that this change will lead to a large drop of hardness. From these we can conclude that in the welding process, the high temperature caused a direct internal transformation from β'' to $U2$, leading to the growth of precipitates in cross section. The strengthening effect of these intermediate precipitates is weaker than fine needle-shaped β'' particles. Consequently, the reason for the softening behavior in HAZ(II) is the dissolution of the majority of short needle-like β'' phases and the direct internal transformation from some larger sized β'' phases to $U2$ phases.

With respect to HAZ(III) (6 mm to 7 mm, 514°C to 560°C), the dissolution of precipitates and the phase transformation process are distinct compared with HAZ(II). From Fig. 7a, the phenomenon of complete disappearance of β'' phases as well as blurry phases/Al boundaries of residual precipitates is more dominant. Due to higher temperatures, this region exhibits more severe dissolution of precipitates than HAZ(II). Furthermore, rod-like β' phases with 68.4 nm to 166.6 nm in length and 8.3 nm to 11.4 nm in diameter as well as plate-like β particles with 60.1 nm to 77.3 nm in edge length and 4.1 nm to 5.2 nm thick were detected. Their density, however, is quite low. Figure 7b shows an embedded β' phase with the rectangular cross section, and its size is about a short-axis length of 5.0 nm and a long-axis length of 15.3 nm. Its long axis parallels to the $\langle 310 \rangle_{Al}$ direction. The unit cell structure and different orientations were outlined in Fig. 7c. The lattice parameter of rod-shaped β' is in accordance with the reported ones as a hexagonal unit structure and lattice parameters of $a = 0.715$ nm and $c = 1.215$ nm.²² The corresponding orientation of β' with the Al matrix can be described as follows:

$$(0001)_{\beta'} \parallel (001)_{Al}, [2\bar{1}\bar{1}0]_{\beta'} \parallel [310]_{Al} \quad (7)$$

Similarly, the fcc unit structure of the β phase and the β -plate/Al orientation relationship were outlined in Fig. 7c. The lattice parameter of the β phase is $a = 0.449$ nm. And the present observed results indicate that the β phase is related to the Al matrix in the relationship as reported by Ohmori et al.:²³

$$(001)_{\beta} \parallel (001)_{Al}, [110]_{\beta} \parallel [010]_{Al}, [1\bar{1}0]_{\beta} \parallel [100]_{Al} \quad (8)$$

Through this analysis, it is supposed that the coexistence of β' and β in HAZ(III) can be attributed to the most possible precipitation sequence in Al-Mg-Si alloys induced by higher peak temperature and the incomplete phase transformation due to the faster heating rate. During MIG welding, coherent β'' phases can directly transform to β' phases by means of atomic diffusion.⁷ Then, as welding temperatures increases, β particles will nucleate at β' rods and grow up by gradually consuming the rods.²⁴ However, because the heating rate ($\sim 47^\circ\text{C s}^{-1}$) in HAZ(III) is substantially faster than regular artificial aging, the phase transformation is not completed, which results in the coexistence of these two phases. To sum up, the softening of HAZ(III) can be explained by the fact that many β'' precipitates are dissolved and low-density β' and β phases are generated from β'' precipitates.

In summary, for the HAZ of the 6082-T6 MIG welded joint, the higher the peak temperature experienced, the more complete the dissolution of the β'' phase precipitates in corresponding subzones. In addition, with the increase in temperatures, there are obvious differences in the phase transformation process for different subzones. The partial or even complete disappearance of β'' phases in the HAZ causes the decrease in mechanical properties. Therefore, the HAZ shows the lowest hardness and the fracture of the tensile specimen (Fig. 2) appeared in this location. Considering together the analysis of precipitation evolution and the minor effect of grain growth on the strength reduction, it has been demonstrated that the mechanism of softening in HAZ is the precipitation evolution rather than grain growth.

Mechanisms of Bake Hardening

Generally, automotive bodies connected by welding require to be baked through three or more cycles. Because of the heat treatability of Al-Mg-Si alloys, paint baking treatments would significantly affect microstructure and mechanical properties of welded Al-Mg-Si joints. The TEM morphology of the precipitates in the subzones of the weld toe and HAZ (III) after three cycles are shown in Fig. 8.

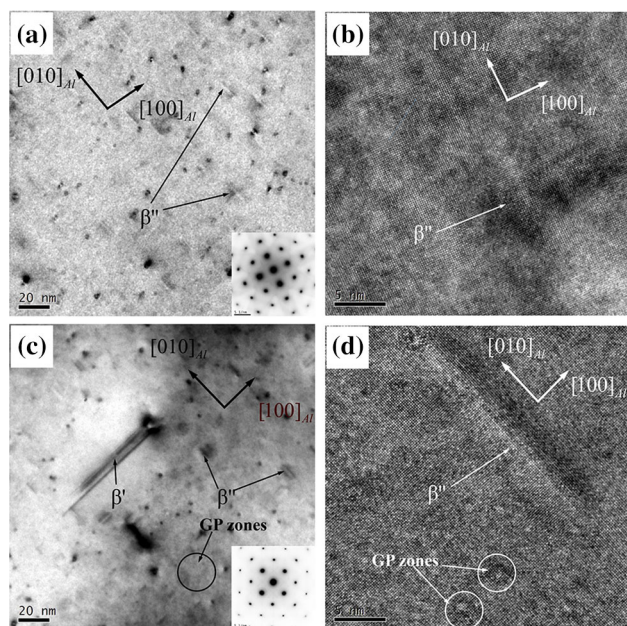


Fig. 8. TEM micrographs (a), (c) and HRTEM image (b), (d) under the $[001]_{Al}$ zone axis of the weld toe (a and b) and HAZ (III) (c and d) of the MIG welded joint baked for three cycles of 30-min baking at $175^{\circ}C$.

This work has confirmed that paint baking can efficiently improve the mechanical properties of 6082-T6 welded joints (Fig. 2). The bake hardening phenomenon can be explained by microstructural analysis of subzones of the weld toe and HAZ(III) baked for three times. For the weld toe, the maximum temperature of this region during welding is $650^{\circ}C$, which is high enough for a complete dissolution of precipitates. After three cycles of the baking treatment, several new needle-like precipitates pointing in the $\langle 100 \rangle_{Al}$ direction considered to be β'' phases were found in this region (Fig. 8a). In contrast to Figs. 7a and 8c, except rod-shaped β' phases generated by welding, there is also an abundance of new GP zones and needle-like β'' precipitates in the HAZ(III). From Fig. 8d, fully coherent relationships between spherical GP zones and Al matrix can be found. These fine and coherent particles like GP zones and β'' precipitates are capable of being sheared by dislocations, indicating the strengthening effect. In the weld toe and HAZ(III), the re-precipitation of GP zones and β'' phases during baking can be ascribed to a high concentration of solute atoms resulting from complete or partial dissolution of precipitates. High temperatures and cooling rates after welding produced the super-saturated solid solution (SSSS).²⁵ Therefore, during paint baking processes, high-concentration solute atoms, such as Mg and Si atoms, will re-precipitate from SSSS to form GP zones and β'' phases. As for HAZ, the hardness increase after three baking cycles is lower than the weld toe. It can be explained from the perspective of the supersaturation level. As stated, the higher

degree of dissolution of precipitates would result in more available solute atoms stored in the Al matrix, indicating the higher supersaturation level. In the HAZ, both peak temperatures and the cooling rate during welding are lower than the weld toe, leading to only partial dissolution of precipitates. Therefore, compared with the weld toe where precipitates have been dissolved fully in the Al matrix, the supersaturation level of the HAZ will be lower, which weakens the hardness response of HAZ regions to paint baking.

CONCLUSION

Precipitation evolution-induced hardness variation in 6082-T6 alloy under multistage heating processes of MIG welding and subsequent paint baking was characterized systematically. Mechanisms of thermal softening during welding and strength recovering in post-weld baking were interpreted. Conclusions can be drawn as follows:

- I. The factor responsible for thermal softening of the HAZ of Al-Mg-Si welded joints is precipitation variation rather than grain growth. The precipitation evolution in diverse subzones can be summarized as the dissolution and coarsening in size of β'' strengthening precipitates and phase transformation from β'' phase to U_2 , β' and β phases.
- II. Post-weld paint baking cycles are capable of improving the performance of the welded joints efficiently owing to the high supersaturation level. The re-precipitation of GP zones and β'' phases from solid solution during baking cycles mainly contributes to the strengthening effect.
- III. The subzone of weld toe was proved to be more sensitive to paint baking than the HAZ in strength recovering. This can be ascribed to the higher super-saturation level of the weld toe in which the peak temperature and cooling rate are higher than the HAZ.

ACKNOWLEDGEMENTS

This work was supported by the National Natural Science Foundation of China (Grant U1664252) and the National Key Research and Development Program of China (Grant 2016YFB0101700).

REFERENCES

1. F. Nturanabo, L.M. Masu, and G. Govender, *Mater. Sci. Forum* 828–829, 485 (2015).
2. G. Çam and G. Ipekoğlu, *Inter. J. Adv. Manuf. Tech.* 91, 1851 (2017).
3. H. Hori, *Weld. Int.* 25, 737 (2011).
4. T.L. Huang, L.F. Shuai, A. Wakeel, G.L. Wu, N. Hansen, and X.X. Huang, *Acta Mater.* 156, 369 (2018).
5. J.R. Croteau, S. Griffiths, M.D. Rossell, C. Leinenbach, C. Kenel, V. Jansen, D.N. Seidman, D.C. Dunand, and N.Q. Vo, *Acta Mater.* 153, 35 (2018).

6. S. Yan, H. Chen, Z. Zhu, and G. Gou, *Mater. Des.* 61, 160 (2014).
7. M.A.V. Huis, J.H. Chen, H.W. Zandbergen, and M.H.F. Sluiter, *Acta Mater.* 54, 2945 (2006).
8. K. Buchanan, K. Colas, J. Ribis, A. Lopez, and J. Garnier, *Acta Mater.* 132, 209 (2017).
9. M.A. Benoit, M.M. Besse, P. Paillard, T. Baudin, R. Louahdi, and H. Paul, in *International Conference on Trends in Welding Research American Society for Metals*, vol. 1045 (2013).
10. O.R. Myhr and Ø. Grong, *Acta Mater.* 48, 1605 (2000).
11. Y.C. Chen, S.F. Liu, D. Bakavos, and P.B. Prangnell, *Mater. Chem. Phys.* 141, 768 (2013).
12. G.I. Kanel, S.V. Razorenov, K. Baumung, and J. Singer, *J. Appl. Phys.* 90, 136 (2001).
13. W.F. Miao and D.E. Laughlin, *Scr. Mater.* 40, 873 (1999).
14. H.L. Wei, J.W. Elmer, and T. Debroy, *Acta Mater.* 126, 413 (2017).
15. E.O. Hall, *Proc. Phys. Soc. B* 64, 747 (1951).
16. N.J. Petch, *J. Iron Steel Inst.* 174, 25 (1953).
17. P. Zhang, S.X. Li, and Z.F. Zhang, *Mater. Sci. Eng. A* 529, 62 (2011).
18. M. Furukawa, Z. Horita, M. Nemoto, R.Z. Valiev, and T.G. Langdon, *Acta Mater.* 44, 4619 (1996).
19. M.A.V. Huis, M.H.F. Sluiter, J.H. Chen, and H.W. Zandbergen, *Phys. Rev. B* 76, 17413 (2017).
20. J.D.D.A. Granholt, *Precipitate Structure Changes During Overaging in an Al-Mg-Si Alloy* (Trondheim: Norwegian University of Science and Technology, 2012).
21. V. Fallah, B. Langelier, N. Ofori-Opoku, B. Raeisinia, and N. Provatas, *Acta Mater.* 103, 290 (2016).
22. S.J. Andersen, H.W. Zandbergen, J. Jansen, C. Traeholt, U. Tundal, and O. Reiso, *Acta Mater.* 46, 3283 (2007).
23. Y. Ohmori, D.L. Chau, Y. Matsuura, S. Kobayashi, and K. Nakai, *Mater. Trans.* 42, 2576 (2001).
24. Y. Ohmori, D.L. Chau, and K. Nakai, *Mater. Trans.* 43, 246 (2002).
25. A. Pogatscher, E. Leitner, and P.J. Uggowitzer, *Acta Mater.* 59, 3352 (2011).

Publisher's Note Springer Nature remains neutral with regard to jurisdictional claims in published maps and institutional affiliations.